Phys Chem Minerals (2003) 30: 185–191
DOI 10.1007/s00269-003-0306-6

ORIGINAL PAPER

P. Lepetit · K. Bente · T. Doering · S. Luckhaus

Crystal chemistry of Fe-containing sphalerites

Received: 25 April 2001 / Accepted: 14 February 2003

Abstract Cell dimensions and solvus properties of Fe-containing sphalerites, depending on temperature and sulfur fugacity, were investigated using equilibrated powdered materials synthesized from elements and binary sulfides under vacuum. The Fe solvus in sphalerite, determined by optical microscopy and microprobe analysis, are directly correlated with increasing temperature and decreasing sulfur fugacity controlled by solid-state buffers. The increase of lattice parameters with Fe correlates with an increase of FeS independent of sulfur fugacity up to 10 mol% FeS within ZnS. Above about 10 mol% the lattice parameters are strongly depending on the sulfur fugacity controlled Fe^{3+}/Fe^{2+} ratios. The Fe^{3+}/Fe^{2+} ratios determined by Moessbauer spectroscopy and involving metal vacancies depend on the sulfur fugacity. The critical Fe^{2+} content determined by experimental simulations as well as the minimal Fe^{3+}/Fe^{2+} ratios agree with the required minimal Fe content for $CuFeS_2$-DIS in sphalerite. The critical Fe^{2+} content also agrees with the change of Moessbauer signal from a singlet to a doublet for Fe^{2+} containing sphalerite. Pyrrhotite exsolutions in sphalerite caused by higher sulfur fugacity show orientationally intergrown with the sphalerite matrix. Density data calculated from lattice parameters and composition are compared with experimental density measurements.

Keywords Sphalerite · (Zn, Fe) S solid solution series · Pyrrhotite exsolutions

P. Lepetit · K. Bente (✉) · T. Doering
Institute for Mineralogy,
Crystallography und Material Sciences,
University of Leipzig,
Scharnhorststr. 20, 04275 Leipzig, Germany
e-mail: bente@rz.uni-leipzig.de

S. Luckhaus
Faculty of Mathematics and Computer Sciences,
University of Leipzig, Augustusplatz10/11,
04109 Leipzig, Germany

Introduction

The use of sphalerite parageneses for the genetic interpretation of sulfide paragenesis requires, besides the knowledge of its chemistry, structure and texture, experimental as well as corresponding mathematical simulations. For interpretational purposes, a huge number of metal substitution data including natural and experimental data exist for Mn, Cd, Cu and In, but especially for Fe (Nelkowski and Bollmann 1969; Moh 1975; Barton and Bethke 1987; Eldridge et al. 1988; Johan 1988; Bente and Doering 1995).

Literature data for geointerpretational use mainly refer to equilibria in the system ZnS–FeS recording temperature–pressure correlations, structural parameters and activity data by means of X-ray diffraction (Barton and Toulmin 1966), Moessbauer and infrared spectroscopy (Manning 1967; Keys et al. 1968; Gerard et al. 1971; Scott 1971) and density determinations (Cabri 1969). These data differ drastically with regard to the occurrence of Fe^{3+} in (Zn, Fe)S (Manning 1967; Keys et al. 1968; Cabri 1969; Gerard et al. 1971; Scott 1971). Systematical investigations referring to the valency of Fe are not known for the solvus compositions of sphalerite, including the sulfur fugacity relations. Gerard et al. (1971) investigated only five sphalerites with different contents of Fe within the range of 0.4 to 62 mol% Fe in ZnS. If the sphalerite contains less than 6 mol% Fe, the Moessbauer spectra shows only a singlet. If the Fe content exceeds 6 mol% a doublet was recorded (Keys et al. 1968; Gerard et al. 1971). Furthermore, literature data for exsolution phenomena produced by the transition of ZnS solvi, especially with chalcopyrite and Fe–S phases, do not explain, for example, the chalcopyrite disease phenomena.

However, these correlations are decisive for the review of substitutional sphalerite equilibria as well as for the kinetics of mineral formation of sphalerite-bearing paragenesis, especially for diffusion-induced segregations (DIS), e.g. of chalcopyrite.

Firstly, Bente and Doering (1993) produced all typical textures of the chalcopyrite or iss disease observed in nature by solid-state diffusion experiments. They have shown that DIS (diffusion-induced segregation) of chalcopyrite or iss respectively, is based on an irreversible process and cannot be explained by solvus transition, e.g. by decreasing temperature. DIS was successfully produced along a chemical potential gradient between Fe-bearing sphalerite and Cu sources controlled by sulfur fugacity and metal activity differences. Primary Fe-bearing sphalerites with more than 5 mol% FeS are required to initiate the DIS process. The increase of the sulfur fugacity results in partial oxidation of Fe^{2+} to Fe^{3+} within the sphalerite (K. Bente and G. Amthauer, personal communications, 1996). Consequently, copper diffusing into spalerite reacts with Fe^{3+} leading to DIS of Cu–Fe–S phases. The corresponding atomistic reaction mechanism is given below starting from (Zn, Fe)S and finishing with DIS of Cu–Fe–S phases.

In addition to earlier assumptions, the results of Bente and Doering (1993) support criticism (Barton and Toulmin 1966) that exsolutions and Fe-bearing sphalerites cannot be used for geothermometry and geothermobarometry, since Fe is depleted and diffuses outside the primary sphalerite, during the formation of Cu-rich DIS phases in sphalerite. Therefore, the original Fe content cannot be recalculated.

Aims

Within the scope of experimental and mathematical simulations of chalcopyrite- or iss diffusion- induced segregation (DIS) within sphalerite, the acquisition of atomistic reaction mechanisms is essential. According to our previous research (Bente and Doering 1993, 1995; K. Bente and G. Amthauer, personal communications, 1996), requirements for the DIS are the content of Fe > 5 mol% in primary sphalerite and the oxidation of Fe caused by the increase of the sulfur fugacity and, additionally, the diffusion of copper into sphalerite and its reaction with Fe^{3+}. Requirements for the mathematical simulation are, besides the knowledge of the driving force, particularly the structural gradients due to local phenomena. In order to estimate these local mechanisms, the correlation between the lattice parameters, the Fe content and the electronic state of different Fe valencies, as well as the sulfur fugacity and thus the Fe^{3+} and vacancy contents, are examined in this study and will be used for calculations of local lattice distortions. The following table of DIS mechanisms shows on an atomistic scale (Table 1) that the correlations of lattice parameters, contents and electronic states of Fe, Fe^{3+}/Fe^{2+} ratios and related metal vacancies, local shrinkages by metal loss of sphalerite and dilatations by incoming Cu, as well as local metal attractions, are needed for the understanding and for mathematical simulations.

Experimental

Single crystals as well as powder materials are required to investigate the parameter correlations. Single crystals $(Zn_{0.8}Fe_{0.2})S$ and $(Zn_{0.87}Fe_{0.13})S$ were produced by chemical vapour transport (CVT) in a temperature gradient between 800 and 720 °C using evacuated silica tubes (diameter 15 mm, length 150 mm) and 3 mg J_2ml^{-1} tube volume. The single crystals were used for density measurements and for additional diffusion experiments.

Homogeneous mixed crystal powders with solid solution compositions of $(Zn_{0.7}Fe_{0.3})S$, $(Zn_{0.75}Fe_{0.25})S$ $(Zn_{0.8}Fe_{0.2})S$, $(Zn_{0.85}Fe_{0.15})S$, $(Zn_{0.90}Fe_{0.10})S$, $(Zn_{0.925}Fe_{0.075})S$, $(Zn_{0.95}Fe_{0.05})S$ and $(Zn_{0.975}Fe_{0.025})S$ were synthesized in evacuated and sealed silica tubes from binary sulfides (purity >99.998%) at 850 °C and quenched. These powders were subjected to three different sulfur fugacity buffers [Fe/FeS, $Fe_{0.97}S$ (po), $Fe_{1-x}S/FeS_2$ (po/py) by tube-

Table 1 Mechanisms of diffusion-induced segregation (DIS) of $CuFeS_2$ in sphalerite; $Cu^{+(\prime)}_{Zn2+}$: Cu^+ on Zn^{2+} site; $Fe^{3+(+)}_{Fe2+}$: Fe^{3+} on Fe^{2+} site; V''_{Fe2+} vacancy on Fe^{2+} site; e^- – *electron*; [*ZnS*] recrystallization; [$CuFeS_2$] DIS

1. Oxidation of Fe in (Zn, Fe)S by fS_2 increase and local shrinkage:

$$2Fe^{2+(x)}_{Fe^{2+}} \Leftrightarrow 2Fe^{3+(*)}_{Fe^{2+}} + 2e^- \quad (1)$$

2. Zn diffusion out of the sphalerite crystal, vacancy formation (V) in ZnS including local shrinkage and recrystallization of Fe-poor sphalerite [ZnS] at the primary sphalerite rim:

$$Zn^{2+(x)}_{Zn^{2+}} + \tfrac{1}{2}S_2 + 2e^- \Leftrightarrow V^{(\prime\prime)}_{Zn^{2+}} + [ZnS] \quad (2)$$

3. Cu diffusion and vacancy occupation by Cu and local dilatation:

$$Cu^+_{diffused} + V^{(\prime\prime)}_{Zn^{2+}} \Leftrightarrow Cu^{+(\prime)}_{Zn^{2+}} \quad (3)$$

4. Cu–Fe clustering before DIS nucleation realized by electrostatical attraction of Cu and Fe:

$$Cu^{+(\prime)}_{Zn^{2+}} + Fe^{3+(*)}_{Fe^{2+}} \Leftrightarrow (Cu + Fe)^{(\prime+*)}_{2Me^{2+}} \quad (4)$$

5. $CuFeS_2$ segregation:

$$(Cu + Fe)^{(\prime+*)}_{2Me^{2+}} + 2S^{2-}_{S^{2-}} \Leftrightarrow [CuFeS_2] \quad (5)$$

Summarizing the partial thermodynamic equations leads to an equilibrium model:

$$\tfrac{1}{2}S_2 + Cu^+ 2[FeS]_{ZnS} \Leftrightarrow Fe^{3+(*)}_{Fe^{2+}} + [CuFeS_2] - DIS \quad \text{if } a[Fe^{3+}]_{ZnS} = a[Cu+]_{DIS}$$

Equilibrium constant K: $\ln K = \frac{1}{[a_{Cu+}]^{1/2} * f1/2S_2}$ q.e.d.

in-tube arrangements] to realize a defined sulfur fugacity at 500 and 700 °C. The corresponding fS_2 vs. temperature data for fS_2 buffers in the system Fe–S are taken from Barton and Toulmin (1964). After annealing, the solid solution series and the buffers were studied by optical microscopy, by powder X-ray diffraction (Seifert XRD 3000, Cu-K_d, GaAs standard) and by microprobe analysis (CAMECA SX 100, standards: ZnS and $CuFeS_2$).

The experimental temperature of 700 °C was chosen in order to obtain possibly high diffusion kinetics and thus equilibrium conditions, while not exceeding the upper stability temperature of the pyrite in the buffer. Our experiments refer to iss-DIS and to ccp-DIS because the chalcopyrite phase transition to intermediate solid solution (iss) occurs at 550 °C. Different diffusion constants at 500 and 700 °C cause a duration of synthesis half a year longer at 500 than at 700 °C. Thus, the results of systematical experiments at 700 °C and, for comparison exemplary data of experiments at 500 °C will be discussed in this paper.

Phase determinations and lattice parameter refinements were carried out with the program DIFFRAC AT (Siemens) and APX 63, respectively. The valency and the ratios of Fe ions were also investigated by Moessbauer spectroscopy (^{57}Co source, fit program HYBRID: Lottermoser et al. 1999). The TEM studies were carried out by means of a Philips CM 200 apparatus.

The decisive differences to former experiments (Barton and Toulmin 1966; Cabri 1969; Scott 1971) are that our experiments were restricted to (Zn, Fe)S solid solutions and the three buffers mentioned above. To check the condition of constant sulfur fugacity during the solid solution synthesis, the buffers as well as the samples were analyzed after the annealing process. If the condition of constant sulfur fugacity was fullfilled, phase determinations, lattice parameter refinements and Moessbauer spectroscopy were carried out on the samples and the experiments accordingly called controlled buffer experiments.

Results

Phase determination by optical and chemical analysis

The chemical composition and homogeneity of the (Zn, Fe)S solid solutions was qualitatively examined by optical microscopy of polished sections. These sections were then used for microprobe analysis by 6 measurements per sample, which confirmed the starting composition of the synthesized powders except for sample ZF30/3 (□ in Fig. 1; Table 2; see Discussion and Conclusion). For CVT single crystals the composition between starting powders and crystals differs. Maximum ZnS–FeS solvus yields about 30 mol% FeS for Fe/FeS buffer fugacities at 700 °C, whereas the po/py buffer revealed only 20 mol% in experiment (Fig. 1). For S fugacities of the Fe/FeS buffer, our results of maximum FeS solution of 52 mol% agree with literature data without S-fugacity control. Exsolution of pyrrhotite (po) within the Fe-rich ZnS was observed in this ZnS sample that was originally synthesized with 30 mol% FeS. Exsolutions were obtained with samples of ≥25 mol% FeS as well.

Lattice parameter data by X-ray powder diffraction

Lattice parameter calculations are based on data collections at 25 °C for homogeneous (Zn, Fe)S solid-solution series in single-phase materials as well as in the two-phase equilibrium. They are correlated with Fe content and Fe^{2+}/Fe^{3+} ratios produced by sulfur fugacities (Fig. 1). The hypothesis based on the atomistic DIS mechanisms and initiating this study is confirmed by the experimental data. They refer to the dependence of the lattice parameter on the Fe content in ZnS for controlled buffer experiments. The lattice parameters increase in relation to the Fe content in ZnS according to the enlarged ionic radii of Fe^{2+} and Cu^{+} and decreasing by the radii of Fe^{3+} and vacancies.

Furthermore, Fig. 1 shows the lattice parameters of Fe-containing ZnS and its dependence on the sulfur fugacity. The lattice parameters decrease with increasing sulfur fugacity above 12 mol% FeS in ZnS (Fig. 1; Table 3). The decreasing lattice constant is a summarizing

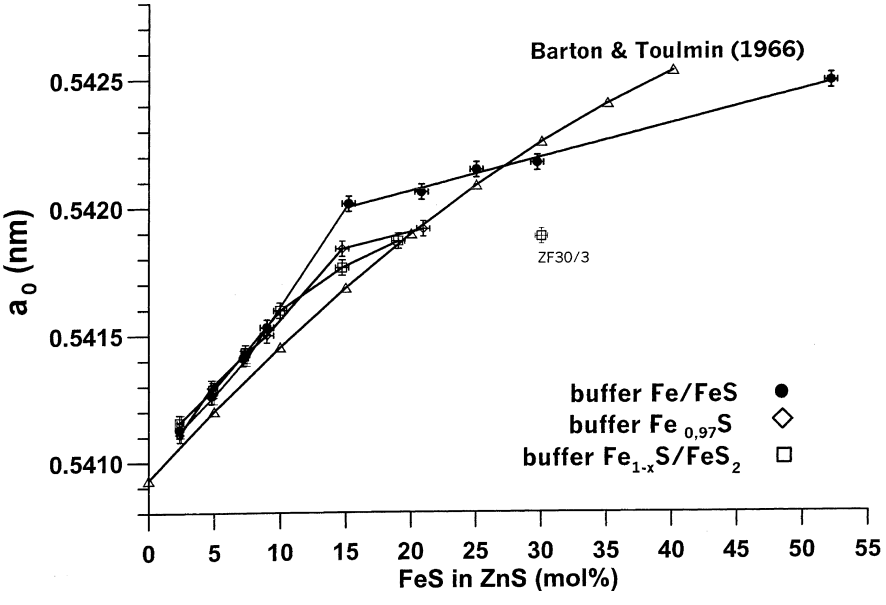

Fig. 1 Correlation between cell parameter and FeS content in ZnS synthesized at 700 °C using buffer 1: Fe/FeS = ●; buffer 2: $Fe_{0.97}S$ = ◇; buffer 3: $Fe_{1-x}S/FeS_2$ = □; Δ = according to the equation given by Barton and Toulmin (1966)

Table 2 Composition of starting materials in comparison to microprobe analysis of synthesized and buffered powders, six measurements per sample

Sample declaration 700 °C	Starting composition $[Zn_{1-x}Fe_x]S$	Buffer	Mean composition of six measurements for each powder sample $[Zn_{1-x}Fe_x]S$
ZF30/1	0.3	Fe/FeS	0.30 ± 0.01
ZF30/3		$Fe_{1-x}S/FeS_2$	0.20 ± 0.01
ZF25/1	0.25	Fe/FeS	0.25 ± 0.01
ZF20/1	0.2	Fe/FeS	0.21 ± 0.02
ZF20/2		$Fe_{0.97}S$	0.21 ± 0.01
ZF20/3		$Fe_{1-x}S/FeS_2$	0.19 ± 0.02
ZF15/1	0.15	Fe/FeS	0.15 ± 0.02
ZF15/2		$Fe_{0.97}S$	0.15 ± 0.02
ZF15/3		$Fe_{1-x}S/FeS_2$	0.15 ± 0.01
ZF10/1	0.1	Fe/FeS	0.09 ± 0.01
ZF10/2		$Fe_{0.97}S$	0.09 ± 0.01
ZF10/3		$Fe_{1-x}S/FeS_2$	0.10 ± 0.01
ZF7.5/1	0.075	Fe/FeS	0.073 ± 0.001
ZF7.5/2		$Fe_{0.97}S$	0.074 ± 0.001
ZF7.5/3		$Fe_{1-x}S/FeS_2$	0.072 ± 0.001
ZF5/1	0.05	Fe/FeS	0.048 ± 0.001
ZF5/2		$Fe_{0.97}S$	0.048 ± 0.001
ZF5/3		$Fe_{1-x}S/FeS_2$	0.049 ± 0.001
ZF2.5/1	0.025	Fe/FeS	0.024 ± 0.001
ZF2.5/2		$Fe_{0.97}S$	0.024 ± 0.001
ZF2.5/3		$Fe_{1-x}S/FeS_2$	0.024 ± 0.001

result of the oxidation of Fe^{2+} to Fe^{3+} and the simultaneous formation of vacancies.

The effect of decreasing is not significant for samples with less than 12 mol% FeS, because the necessary lattice parameter-reducing amount of Fe^{3+} is not reached yet, which is confirmed by Moessbauer data and will be discussed later. The resolution of data at about 10 mol% FeS in ZnS is too close to the limit of accuracy.

First results of comparing 500 °C samples show the same tendency as at 700 °C. Maximum ZnS–FeS solvus yields about 19 mol% FeS for $Fe_{0.97}S$ buffer at 500 °C.

Table 3 Lattice parameter data for $Zn_{0.8}Fe_{0.2}S$, calculated X-ray density data based on Fe^{2+}/Fe^{3+} ratios and vacancy contents corresponding to Moessbauer spectroscopy data (Table 4), log fS_2 is calculated for 700 °C from Barton and Toulmin (1966)

$[Zn_{1-x}Fe_x]S$	Buffer	Log fS_2	a_0 in nm	ρ (X-ray) theor. (g cm^{-3})
700 °C	Without	Without	0.54189 (1)	3.9870 (1)
	Fe/FeS	−11.4 (5)	0.54206 (1)	3.9834 (1)
$x = 0.2$	$Fe_{0.97}S$	−4.9 (5)	0.54191 (2)	3.9723 (2)
	$Fe_{1-x}S/FeS_2$	−0.97 (5)	0.54187 (1)	3.9684 (1)

Electronic states and valency data of Fe within (Zn,Fe)S by Moessbauer spectroscopy

The valency and ratios of ionic Fe species of single- and two-phase powder materials were determined by Moessbauer spectroscopy. Within the single phase solid solutions of 20 mol% FeS, the Fe^{3+} content increases from 0 to 5.4% and up to 7.3 mol% with increasing sulfur fugacities from the Fe/FeS buffer – through the po buffer – to the po/py buffer (Table 4).

In one non-equilibrium powder sample of a (Zn,Fe)S solid-solution series, two signals with identical isomer shift (0.65 mm s^{-1}, corrected to d-Fe) were obtained. One signal shows a quadrupole split of 0.60 mm s^{-1}, whereas the other shows only a singlet (Fig. 2; Table 5). The different signals correspond to two different solid-solution members $(Zn_{0.93}Fe_{0.07})S$ and $(Zn_{0.88}Fe_{0.12})S$ determined by microprobe analysis. Because at the given fS_2 only Fe^{2+}-containing sphalerite exists, the singlet–doublet transition has to be attributed to a Fe–Fe-bonding interaction above a critical Fe content in ZnS. This transition from singlet to doublet spectra agrees with the value for minimal Fe contents in sphalerite producing $CuFeS_2$ DIS. Additionally, small amounts of pyrrhotite were detected by microscopy and microprobe analysis, but do not contribute to the Moessbauer signals.

Density data

Local shrinkage due to changes in valency state (Fe^{2+}/Fe^{3+}) and the formation of vacancies was examined by

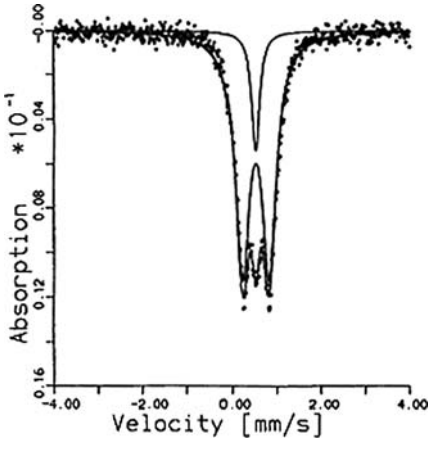

Fig. 2 Fitted Moessbauer spectra with two signals at identical isomer shift

Table 4 Increasing content of Fe^{3+} in $(Zn_{0,8}Fe_{0,2})S$ caused by increasing sulfur fugacity (buffer controlled experiments)

$[Zn_{1-x}Fe_x]S$ 700°C	Buffer	Fe^{3+} (%)	IS (mm/s^{-1})	QS (mm/s^{-1})	Fe^{2+} (%)	IS (mm/s^{-1})	QS (mm/s^{-1})
x = 0.2	Fe/FeS	0	–	–	100	0.64	0.49
	$Fe_{0.97}S$	5.4	0.36	0.17	94.6	0.64	0.43
	$Fe_{1-x}S/FeS_2$	7.3	0.39	0.20	92.7	0.66	0.44

density calculations. Density data were calculated on the basis of the refined lattice parameters. The results of the maximum Fe^{3+} content causing simultaneously an amount of vacancies being half of the Fe^{3+} in order to maintain charge balance (Table 1, 3). The type of lattice distortion caused by the vacancies is reducing because of the ionic bonds in (Zn, Fe)S. The calculated density variations correlate with the lattice data. The calculated densities for the buffered $Zn_{0.8}Fe_{0.2}S$ compared to $Zn_{0.8}Fe_{0.2}S$ without buffering (Table 3), that means $Zn_{0.8}Fe_{0.2}S$ only containing Fe^{2+}, vary up to about 0.5%. These estimated differences will be examined in a future experiment by using buffered (Zn, Fe)S single crystals.

Microstructural data by TEM

The coexistences of (Zn, Fe)S with exsolved Fe–S phases were investigated to determine the solvus limits. Hereby the solid solution limits of FeS in ZnS at 700 °C are 52 mol% for the Fe/FeS buffer, 21 mol% for the $Fe_{0.97}S$ buffer and 20 mol% for the $Fe_{1-x}S/FeS_2$ buffer. Pyrrhotite exsolution was detected at 25 and 30 mol% at the $Fe_{0.97}S$ and at the Fe_{1-x}/FeS_2 buffer.

TEM studies of the pyrrhotite exsolutions showed (Fig. 3) an orientation of the pyrrhotite {0001} parallel to {111} of the sphalerite matrix. The exsolutions (black, rounded phase) are abundantly surrounded by dislocations (D in Fig. 3) in the matrix. Figure 4a, b shows calculated diffraction patterns of pyrrhotite and sphalerite. The comparison between computer simulated (EMS Stadelmann program) and experimental diffraction pattern confirmed pyrrhotite as second phase. The superposition of both diffraction patterns (po and sph) produces a diagram which is almost identical to the experimental observed pattern (Fig. 4c) and its orientation correlation. The pyrrhotite modification showing the best agreement was obtained with Fe_7S_8 (trigonal).

Fig. 3 Relation between pyrrhotite exsolution and sphalerite matrix. Multibeam TEM bright-field image (bd = [111]) with corresponding diffraction pattern (SADP) for the sphalerite matrix and pyrrhotite as well as for dislocations (*D*). Sample LZF 30/3, Philips CM 200, U = 200 kV

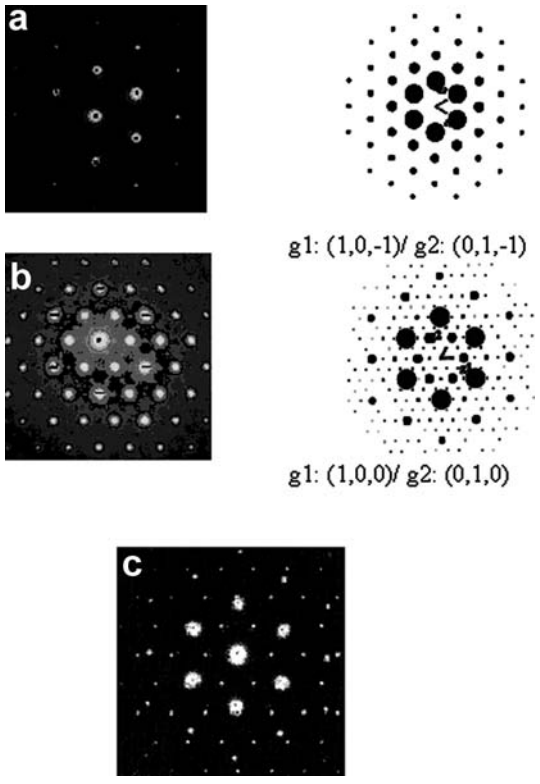

Fig. 4a–c Relationship between calculated and experimental diffraction patterns of $Fe_{1-x}S$ and ZnS for the beam directions $bd_{(ZnS)} = [111]$ and $bd_{(Fe1-xS)} = [0001]$. **a** Sphalerite. **b** Pyrrhotite. **c** Superposition of both diffraction patterns

Discussion

The X-ray data of Fe-containing sphalerite reveal a correlation between the dependence of sulfur fugacity, the lattice parameters, the Fe^{3+} and vacancy concentration. These data specify and correct literature data of sphalerite-FeS solid solutions which are predominantly studied without strictly controlled S fugacities and indicate that this system is sensitive to the experimental procedures. Barton and Toulmin (1966) investigated the buffers after completing their experiments. "Various pyrrhotite solid solution buffers" (> Fe/FeS, p. 822) were responsible for their lattice parameters and explain why their regression line plots differently to our data. In the range between $(Zn_{0.975}Fe_{0.025})S$ and $(Zn_{0.90}Fe_{0.1})S$ the slope of both lines is almost parallel. At higher Fe contents the effect of Fe^{3+} and vacancies leads to a splitting of our line caused by controlled fS_2 and confirms our atomistic model (Table 1).

Table 5 Isomer shift and quadrupol splitting of the two-phase sample

$[Zn_{1-x}Fe_x]S$	IS (mm/s^{-1})	QS (mm/s^{-1})
0.07 ± 0.01	0.65	0
0.12 ± 0.01	0.65	0.60

The preparation of materials excluded pyrrhotite as starting and coexisting phase with (Zn, Fe)S. Pyrrhotite exsolutions (sample ZF30/3) indicate that the maximum solubility of FeS in ZnS is achieved with the $Fe_{1-x}S/FeS_2$ buffer. It has to be assumed that it presents the upper solubility limit. According to our experiments the maximum solubility of FeS in ZnS yields about 21 (±2) mol% FeS for the $Fe_{1-x}S/FeS_2$ buffer. As a result of these data and of the fact of pyrrhotite exsolution within sphalerite at 25 and 30 mol% FeS in ZnS, diffusion experiments will further be focused on the solubility range from $(Zn_{0.075}Fe_{0.025})S$ to $(Zn_{0.80}Fe_{0.20})S$. The regression for the Fe/FeS buffer at 52 ± 1 mol% FeS represents the maximum FeS solubility in ZnS under these conditions.

Furthermore, the observed exsolutions of pyrrhotite are useful for investigations referring to the characterization of lattice distortions.

Moessbauer spectra of Fe-containing sphalerites are known from literature. Gerard et al. (1971) investigated five (Zn, Fe)S samples within the range of 0.4 to 62 mol% Fe in ZnS. If the sphalerite contains less than 6 mol% Fe, the spectra show only singlets. If the Fe content exceeds 6 mol%, it shows a doublet (Keys et al. 1968; Gerard et al. 1971). These data agree with our data (7 ± 1 mol%). Scott (1971) investigated samples with 20.8 up to 43.6 mol% Fe in ZnS, which explains why he did not obtain a singlet. In a non-equilibrium experiment, different Fe-rich sphalerites could be measured simultaneously. It has to be assumed that in this case of a singlet, the Fe ions are in the state of low spin and thus show no interaction, but in the case of more Fe-rich phases, the Fe ions are in the condition of high spin and interactions take place and the signal changes to a doublet. The obtained α-Fe corrected data of isomer shift of Fe-containing ZnS (0.65 mm s^{-1}) agree with literature data (Manning 1967; Gerard et al. 1971; Scott 1971). The change in the Moessbauer signal (between 7 and 12 mol% FeS in ZnS) agrees with the splitting of the lattice parameters starting at about 10 mol% FeS in ZnS.

Discussions about possibly ordering phenomena depending on the Fe content, leading to these Moessbauer signals, will be proved by neutron diffraction. First results by neutron diffraction (Schorr 2002, personal communication) confirm lattice parameter data obtained by X-ray diffraction.

The existence of Fe^{3+} within (Zn, Fe)S is described in literature. Gerard et al. (1971) mentioned detection of Fe^{3+} in "small amounts" (p. 2093) in Fe-rich ZnS, but their research did not focus mainly on Fe^{3+}. Bente and Amthauer measured Fe^{3+} in (Zn, Fe)S and confirmed literature data. The splitting of the regression line of the lattice parameter into three lines with different slopes is caused by the oxidation of Fe^{2+} to Fe^{3+} and the simultaneous formation of vacancies depending on the sulfur fugacity. Obviously, the critical Fe^{2+} content and the minimal Fe^{3+}/Fe^{2+} ratios agree with the required minimal Fe content for $CuFeS_2$-DIS in sphalerite.

Conclusions

The lattice parameters of ZnS–FeS solid solutions, depending on temperature and sulfur fugacity, verify the hypothesis that increasing Fe content and decreasing sulfur fugacity reveal an increase in the cell dimensions. The increase in S- fugacity implies the increase in Fe^{3+}. The observed solid solutions can be used for solvus phenomena as well as for the starting conditions and mechanisms of diffusion-induced segregations, e.g. of chalcopyrite.

The critical composition of (Zn, Fe)S that results in quadrupole splitting of Moessbauer spectra corresponds with the experimentally determined minimum content of Fe required for chalcopyrite- or iss- DIS in sphalerites. The interaction of Fe above ca. 7 mol% FeS in sphalerite obtained by Moessbauer spectroscopy is an essential requirement for the formation of Cu–Fe clusters precursing DIS nucleation. Additionally, it has to be assumed that for FeS contents below and above 7 mol% in sphalerite, different diffusion mechanisms could be suggested.

Further systematic studies will include experimental investigations into local shrinkage and at temperatures differing from 700 °C by means of experimentally determined densities of crystals with high precision. These local shrinkage data are used for mathematical simulation of DIS (Blesgen et al. 2002).

Acknowledgements Our thanks go to Dr. G. Wagner (Institute of Surface Modification, Leipzig) for TEM images and Dr. W. Lottermoser (University of Salzburg) for measurements and discussions of Moessbauer data. This work is funded by the Deutsche Forschungsgemeinschaft (DFG) under Lu 312/6 within the Schwerpunktprogramm Strukturgradienten.

References

Barton PB, Bethke PM (1987) Chalcopyrite disease in sphalerite: pathology and epidemology. Am Mineral 72: 451–467

Barton PB, Toulmin P III (1964) The electrum-tarnish method for the determination of the fugacity of sulfur in laboratory sulfide systems. Geochim Cosmochim Acta 28: 619–40

Barton PB Jr, Toulmin P III (1966) Phase relations involving sphalerite in the Fe–Zn–S system. Econ Geol 61: 815–849

Bente K, Doering Th (1993) Solid-state diffusion in sphalerites: an experimental verification of the "chalcopyrite disease". Europ J Mineral 5: 465–478

Bente K, Doering Th (1995) Experimental studies on the solid-state diffusion of Cu + In in ZnS and on "disease", DIS (diffusion

induced segregations), in sphalerite and their geological applications. Mineral Petrol 53: 285–305

Bente K, Doering Th, Lepetit P, Luckhaus S, Lehmann S, Fleischer F, Wagner G (2001) Kristallchemie und Metrik Fe-haltiger Zinkblenden bei der diffusionsinduzierten $CuFeS_2$-Segregation (DIS). DMG (Deutsche Mineralogische Gesellschaft) Congress Potsdam (2001)

Blesgen T, Luckhaus S, Bente B (2002) Modeling and numerical simulation of diffusion induced segregation. Crystallogr Res Technol 37: 570–580

Cabri LJ (1969) Density determinations: accuracy and application to sphalerite stoichiometry. Am Mineral 54: 539–548

Eldridge CS, Bourcier WL, Ohmoto H, Barnes HL (1988) Hydrothermal inoculation and incubation of the chalcopyrite disease in sphalerite. Econ Geol 83: 978–989

Gerard A, Imbert P, Prange H, Varret F, Winterberger M (1971) Fe^{2+} impurities, isolated and in pairs, in ZnS and CdS studied by the Mößbauer effect. J Phys Chem Solids 32: 2091–2100

Johan Z (1988) Indium and Germanium in the structure of sphalerite: an example of coupled substitution with copper. Mineral Petrol 39:211–229

Keys JD, Horwood JL, Baleshta TM, Cabri LJ, Harris DC (1968) Iron–iron interaction in iron-containing zinc sulphide. Can Mineral 9: 453–467

Lepetit P, Bente K, Luckhaus S, Klöß G (2000) Strukturgradienten während Diffusionsinduzierter Segregationen (DIS) im System (Zn, Fe)S – $CuFeS_2$. Abstract, DMG (Deutsche Mineralogische Gesellschaft) Congress Heidelberg (2000)

Lottermoser W, Schell T, Steiner K, Amthauer G (1999) A time-minimizing hybrid method for fitting complex Mössbauer spectra. Abstracts ICAM (Int. Congr. Appl. Mineralogy) E99 Garmisch-Partenkirchen, T9/33

Manning PG (1967) Absorption spectra of Fe(III) in octahedral sites in sphalerite. Can Mineral 9: 57–64

Moh GH (1975) Tin-containing mineral systems, Part II: Phase relations and mineral assemblages in the Cu–Fe–Zn–Sn–S system. Chemie Erde 34: 1–61

Nelkowski H, Bollmann H (1969) Diffusion von In und Cu in ZnS-Einkristallen. Z Naturforschg (A)24: 1302–1306

Scott SD (1971) Mößbauer spectra of synthetic iron-bearing sphalerite. Can Mineral 10: 882–885